Action Potential Duration Restitution Portraits of Mammalian Ventricular Myocytes: Role of Calcium Current

Elena G. Tolkacheva, Justus M. B. Anumonwo, and José Jalife
Department of Pharmacology, Institute for Cardiovascular Research, State University of New York Upstate Medical University, Syracuse, New York 13210

ABSTRACT Construction of the action potential duration (APD) restitution portrait allows visualization of multiple aspects of the dynamics of periodically paced myocytes at various basic cycle lengths (BCLs). For the first time, we obtained the restitution portrait of isolated rabbit and guinea pig cardiac ventricular myocytes and analyzed the time constant, τ, of APD accommodation and the slopes of different types of restitution curves, S_{dyn} and S_{12}, measured at varying BCLs. Our results indicate that both τ and the individual slopes are species and pacing dependent. In contrast, the mutual relationship between slopes S_{dyn} and S_{12} does not depend on pacing history, being a generic feature of the species. In addition, the maximum slope S_{12}, measured in the restitution portrait at the lowest BCL, predicts the onset of alternans. Further, we investigated the role of the L-type calcium current, $I_{Ca\text{-}L}$, in the restitution portrait. We found that $I_{Ca\text{-}L}$ dramatically affects APD accommodation, as well as the individual slopes S_{dyn} and S_{12} measured in the restitution portrait. However, peak calcium current plays a role only at small values of BCL. In conclusion, the results demonstrate that the restitution portrait is a powerful technique to investigate restitution properties of periodically paced cardiac myocytes and the onset of alternans, in particular. Moreover, the data also show that $I_{Ca\text{-}L}$ plays a crucial role in multiple aspects of cardiac dynamics measured through the restitution portrait.

INTRODUCTION

Electrical restitution plays a vital role in heart function: for a given heart rate, a shorter action potential duration (APD) allows for a longer diastolic interval (DI), thereby giving adequate time for the heart to refill with blood. Although important for life at moderate heart rates, at higher rates restitution may result in life-threatening cardiac rhythms (1–5) such as the beat-to-beat variation of APD, known as alternans. A common technique for studying the initiation and maintenance of alternans and other complex rhythms is to analyze the restitution curve (RC), which expresses the nonlinear functional relation between APD and the preceding DI (6,7). Specifically, it was proposed (6,7) that the slope of the RC might be related to the onset of alternans. However, assessment of the role of restitution in the onset of cardiac arrhythmias has produced mixed results (8), particularly because of the existence of memory in the cardiac response, i.e., the dependence of APD on activating history, not only the preceding DI. Memory gives rise to rate-dependent restitution (9,10), which means that the RC depends on the pacing protocol. Currently, several protocols are used to measure different types of RCs, each of which measures an individual RC, where the dynamic and the *S1-S2* RCs are the most common (11). Typically, these RCs have different slopes and none of them predicts the onset of alternans correctly (9,12–15).

The first attempt to systematically measure the RC was done in Tolkacheva et al. (16) and Kalb et al. (17) where the perturbed downsweep protocol (PDP) was proposed to simultaneously measure a combination of different RCs at each basic cycle length (BCL), instead of individual RCs. The PDP allows one to construct the restitution portrait of periodically paced cardiac tissue, which will enable the visualization of multiple aspects of cardiac dynamics, such as the slopes of different RCs and the APD accommodation effect at various values of BCL.

A variety of ionic currents underlie the action potential (AP) in different species. However, the ionic mechanisms underlying electrical restitution are not clear. A number of experimental and simulation studies investigated AP properties of periodically paced cardiac tissue (18–22). For example, it was proposed that adaptation of APD to cycle length change could be attributed to the recovery kinetics of different ionic currents or to changes in intracellular and extracellular ion concentrations (18). In contrast to the RC, the restitution portrait is a convenient way to investigate the ionic mechanisms underlying multiple aspects of cardiac dynamics (23). It also may be used as a tool to investigate ionic mechanisms of species-dependent differences in cardiac dynamics.

Here we have systematically analyzed restitution portraits of isolated cardiac myocytes obtained from two mammalian species—the rabbit and the guinea pig—that have different underlying ionic mechanisms. We characterized and compared various aspects of the cardiac dynamics, such as slopes of different RCs and the APD accommodation effect, in both species at different pacing rates. We investigated whether restitution portraits of isolated guinea pig and rabbit

Submitted February 23, 2006, and accepted for publication June 22, 2006.

Address reprint requests to Elena G. Tolkacheva, State University of New York Upstate Medical University, 750 Adams St., Rm. 6301C, Syracuse, NY 13210. Tel.: 315-464-7958; E-mail: talkacal@upstate.edu.

0006-3495/06/10/2735/11 $2.00

doi: 10.1529/biophysj.106.083865

myocytes are qualitatively and/or quantitatively similar. Also, even though the mechanisms underlying any potential quantitative species-dependent differences in the restitution portraits are very interesting and important of themselves, we decided to start by investigating the species-independent ionic mechanisms underlying multiple aspects of cardiac dynamics in the restitution portrait. In particular, in this study we characterize the role of the calcium current in the restitution portrait obtained from isolated rabbit myocytes.

METHODS

Solutions

For myocyte isolation we used the following solutions: Low calcium Tyrode's solution (in mmol/L): NaCl 148, KCl 5.4, $MgCl_2$ 1, NaH_2PO_4 0.4, glucose 5.5, and HEPES 15 (pH 7.2 adjusted with NaOH). Bovine serum albumin (1 mg/ml) was added to this solution. The enzyme was the same as the low calcium Tyrode's solution, except that collagenase type II was added (100 units/ml for guinea pig, 200 units/ml for rabbit; Worthington Biochemicals, Lakewood, NJ). KB solution (mmol/L): KCl 80, $MgSO_4$ 5, KH_2PO_4 30, glucose 20, β-hydroxybutyric acid (sodium salt) 5, creatine 5, ATP 5, taurine 20, EGTA 0.25, pyruvic acid 5.

The standard Tyrode's solution contained the following (in mmol/L): NaCl 148, $CaCl_2$ 1.8, KCl 5.4, $MgCl_2$ 1.0, NaH_2PO_4 0.4, glucose 5.5, and HEPES 15 (pH 7.4 adjusted with NaOH). This solution was used for cell isolation and as extracellular solution for AP studies. The pipette solution for the ruptured patch contained the following (in mmol/L): K-aspartate 90, KCl 20, KH_2PO_4 10, EGTA 5, HEPES 5, K_2ATP 1.9. The pipette solution for the perforated patch contained the following (in mmol/L): K-aspartate 140, NaCl 5, MgATP 5, EGTA 1, HEPES 10. After being dipped for ~10 s into the pipette solution, the pipette was then back-filled using the same solution containing 240 μg/mL amphotericin-B (Sigma, St. Louis, MO; catN A4888).

To block L-type calcium current ($I_{Ca\text{-}L}$), nisoldipine (1 μmol/L) was added to Tyrode's solution. To study the effect of extracellular Ca^{2+} cycling, thapsigargin (200 nmol/L) and ryanodine (10 μmol/L) were added to Tyrode's solution.

The extracellular solution for calcium current (I_{Ca}) studies contained the following (in mmol/L) (24): tetraethylammonium-Cl 133, CsCl 5.4, $MgCl_2$ 1, CaCl 2, NaH_2PO_4 0.33, Dextrose 10, and HEPES 10 (pH 7.4 adjusted with CsOH). The pipette solution for I_{Ca} recording contained the following (in mmol/L): CsCl 130, $MgCl_2$ 5, EGTA 10, GTP 0.1, Mg_2ATP 5, Na_2-phosphocloline 5.

Myocyte isolation

Cardiac myocytes were isolated using the Langendorff retrograde perfusion method as previously described (25,26). Adult animals of either sex (rabbits, 1.5–3 kg; guinea pigs, 0.27–0.3 kg) were injected with heparin sulfate (300–500 units) and anesthetized with sodium pentobarbital (rabbits: 75 mg/kg i.v.; guinea pigs: 400 mg/kg i.p.). Hearts were quickly removed, immersed in cardioplegic solution and retrogradely perfused with Tyrode's solution (at 37°C) for ~8 min at 32 mL/min (rabbits) or ~5 min at 16 mL/min (guinea pigs) to remove any excess blood in the vessels. The hearts were then perfused with Ca^{2+}-free Tyrode's solution for 10–12 min, followed by a 10-min (guinea pigs) or a 40-min (rabbits) perfusion with the enzyme solution. Finally, the hearts were perfused with the recovery (KB) solution. Subsequently, strips of tissue were carefully shaved off the left and the right endocardial surfaces of each heart. The tissue strips from each ventricle were separated into tubes containing the KB solution and were mechanically agitated to free the myocytes. After a recovery period of ~30 min, the KB solution was gradually (~20 min) exchanged with normal Tyrode's solution. All experiments were performed at 37°C ± 1°C.

Electrophysiology and data analysis

APs (Part I) and peak I_{Ca} were measured under current and voltage-clamp conditions, respectively, using the ruptured patch configuration of the patch-clamp technique (Figs. 1–4 and 7–9). APs (Part II) to study the effects of inhibiting of $I_{Ca\text{-}L}$ and intracellular Ca^{2+} cycling were measured using the whole-cell perforated patch technique (28) (Figs. 5 and 6). Borosilicate glass electrodes were pulled with a Brown-Flaming puller (model P-97), yielding a tip resistance of 3–5 MΩ when filled with pipette solution. Data were recorded with the use of an Axoclamp-2A amplifier and pClamp8 suite of programs (Axon Instruments, Union City, CA). Stimulus pulses were generated by PCI-6013 Basic Multifunctional I/O board (National Instruments, Austin, TX). A custom-written LabView program (National Instruments) controlled stimulation. APs were elicited by 5-ms stimuli at approximately twice the threshold pulse amplitude. APD was measured at 80% of full repolarization. AP measurements were started ~2 min after patch rupture. Data were sampled at the rate of 20 kHz, filtered, and then stored on the hard disk of an IBM computer.

Group data are presented as mean ± SE unless otherwise stated. Nonlinear curve fitting was performed using Origin software (Origin 7.0,

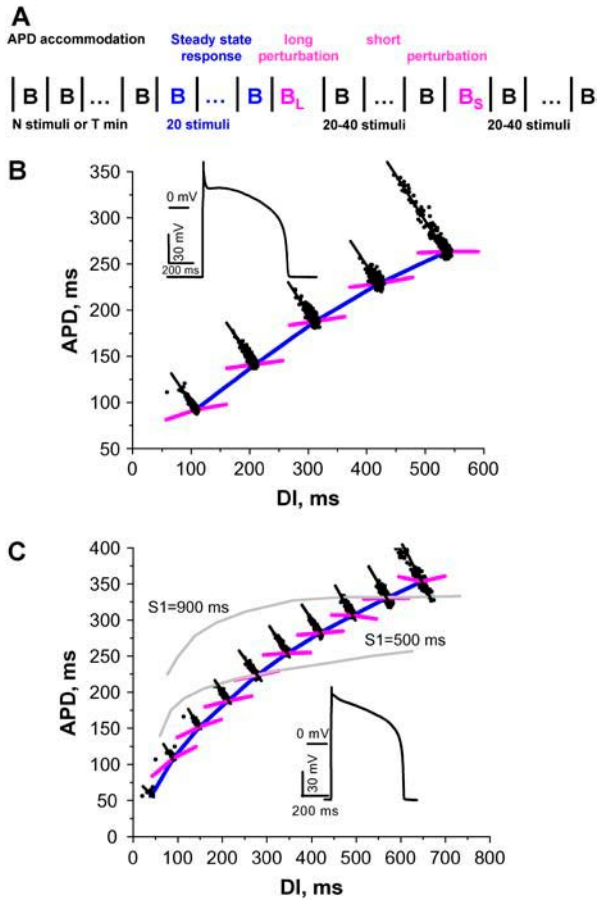

FIGURE 1 Stimulation protocol (*A*) that was used to record restitution portraits of isolated rabbit (*B*) and guinea pig (*C*) myocytes with ruptured patch AP clamp technique. In *A*, only one segment of *PDP* for one value of BCL (*B*) is shown. In *B* and *C*, three different responses are present at each value of BCL: APD accommodation (*black*), dynamic RC (*blue*), and local S1-S2 RCs (*purple*). Note that different colors in stimulation protocol *A* match with recorded responses in *B* and *C*. In *C*, gray traces represent conventional S1-S2 RCs recorded for different values of S1 (S1 = 900 ms and 500 ms). Insets demonstrate rabbit and guinea pig AP profiles.

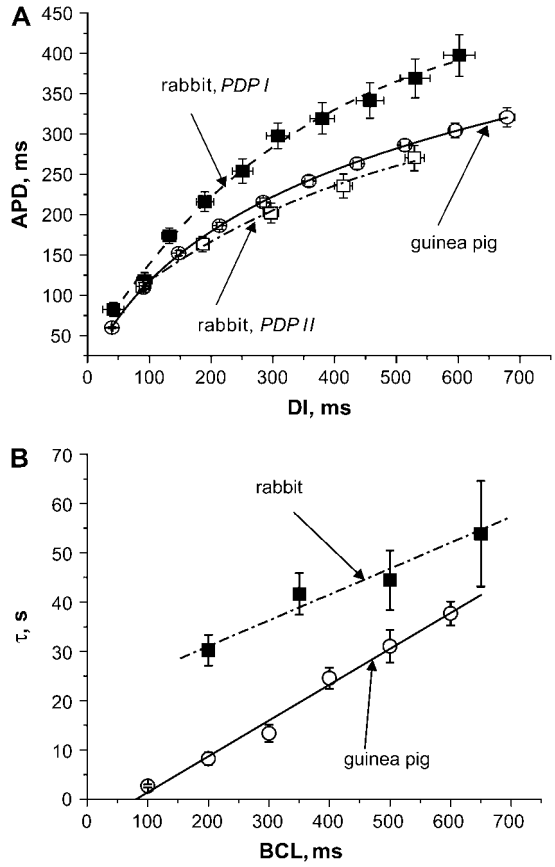

FIGURE 2 (*A*) Dynamic RCs for rabbit and guinea pig myocytes obtained using ruptured patch AP clamp technique for different stimulation protocols: *PDP I* (*solid squares*) and *PDP II* (*open squares*) for rabbit and *PDP III* (*open circles*) for guinea pig myocytes. (*B*) Time constant, τ, of APD accommodation as a function of BCL for rabbit (*solid squares*) and guinea pig (*open circles*) isolated myocytes.

Northampton, MA). Statistical comparisons among groups were performed by ANOVA. Statistical significance is considered as $p < 0.05$.

Pacing protocols

Current-clamp mode

The PDP was first proposed theoretically (16) and later implemented experimentally (17). Briefly, the whole PDP consists of segments of external stimuli. The responses (APD and preceding DI pair) to a given stimulus and several segments of the PDP can be recorded by changing BCL in a downsweep (from largest to smallest value) until achieving a stable 1:1 response. Each segment consists of sequences of stimuli combined in a certain order, as presented in Fig. 1 *A*. The sequence at each BCL consists of the following steps:

I. N stimuli (or T min of pacing) are applied at BCL B to achieve a steady state.
II. Twenty additional stimuli are applied at the same BCL B to measure the steady-state response.
III. One additional stimulus (long perturbation) is applied at a longer BCL $B_L = B + \delta$ ms.
IV. 20–40 stimuli are applied at BCL B to reach a steady state after the long perturbation.
V. One additional stimulus (short perturbation) is applied at shorter BCL $B_S = B - \delta$ ms.
VI. From 20 to 40 stimuli are applied to reach a steady state after the short perturbation.

After completion of I–VI at BCL B, BCL is then decreased by Δ ms, and steps I–VI are repeated.

We used four modifications of the PDP: two for rabbit and two for guinea pig myocytes:

1. *PDP I* (animals = 3, cells = 10) for rabbit: $N = 150$, BCL was changed from 1000 ms to 100 ms with $\Delta = 100$ ms, $\delta = 50$ ms.
2. *PDP II* (animals = 7, cells = 22) for rabbit: $T = 3$ min or $N = 400$, BCL was changed from 800 ms to 200 ms with $\Delta = 150$ ms, $\delta = 50$ ms.
3. *PDP III* (animals = 3, cells = 10) for guinea pig: $N = 200$ or 100, BCL was changed from 1000 ms to 100 ms with $\Delta = 100$ ms, $\delta = 50$ ms.
4. *PDP IV* (animals = 5, cells = 30) for guinea pig: $N = 200$, BCL was changed from 500 ms to 150 ms with $\Delta = 50$ ms; after that BCL was changed from 150 ms to 50 ms with $\Delta = 10$ ms, $\delta = 10$ ms.

The above four modifications were used as a compromise between 1), the number of stimuli that must be applied at a given BCL to reach steady state, and 2), the limited lifetime of the isolated myocyte subjected to periodic pacing (which is ~20–40 min). On the one hand, the more stimuli were applied during step I of the PDP, the more accurately the steady state could be reached. On the other hand, with more stimuli at each BCL, the possibility was greater for cell death before completion of the PDP. Thus, *PDP I* was more focused on obtaining the whole downsweep without loosing a cell, whereas the *PDP II* was aimed at reaching the steady state at each BCL during the downsweep. Our results indicate that isolated guinea pig myocytes reach the steady state more quickly than rabbit myocytes, and thus *PDP III* is similar to *PDP I*. *PDP IV* was designed to approach the onset of alternans very accurately by changing BCL in small steps.

The long duration of the PDP might be inconsistent with the lifetime of some cells and also cause unforeseen current rundown effects. To ensure that current rundown does not occur, the initial part of the PDP was repeated at the end of each experiment to reproduce the initial results.

Voltage-clamp mode

Two different protocols were used in the voltage-clamp mode to measure the peak I_{Ca} in rabbit ventricular myocytes:

AP clamp (*3 rabbits, 12 cells*). To measure the peak I_{Ca} (both L-type and T-type) at steady state, long and short perturbations in the restitution portrait we use AP profiles recorded from steps II–VI of the *PDP II* for BCL = 800, 650, 500, 350, and 200 ms (train of 63 AP profiles in each case). During these protocols, both reactivation and inactivation kinetics of I_{Ca} changed with frequency after frequency-dependent changes in AP profiles.

Voltage steps (*3 rabbits, 10 cells*): To determine the frequency dependence of I_{Ca} we used trains of 10 300-ms square pulses from −80 to +10 mV, with varying intervals between pulses (from 800 to 200 ms). Note that in this conventional voltage-step protocol, the duration of step pulses remains constant. In other words, this protocol is designed to examine frequency-dependent reactivation of I_{Ca} in the absence of changes in the inactivation kinetics.

RESULTS

Part 1: restitution portraits

Characteristics of different responses

Fig. 1 shows representative restitution portraits of isolated rabbit and guinea pig myocytes (*B* and *C*, respectively). The respective insets illustrate typical AP profiles for each

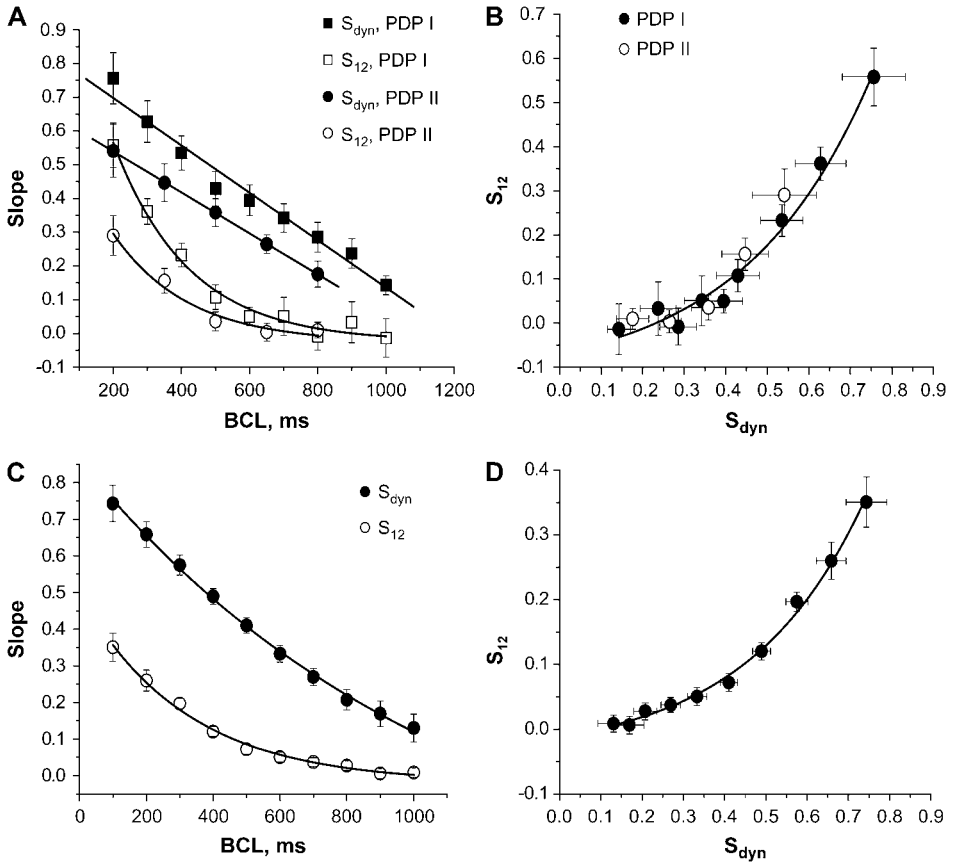

FIGURE 3 Slopes S_{dyn} (*solid symbols*) and S_{12} (*open symbols*) measured from the restitution portraits of the (*A*) rabbit and (*C*) guinea pig myocytes as functions of BCL. In *A*, two different modifications of *PDP* were used: *PDP I* (*squares*) and *PDP II* (*circles*). The relationship between S_{dyn} and S_{12} for (*B*) rabbit and (*D*) guinea pig myocytes. Note that this relationship does not depend on pacing history: in *B*, data obtained using different *PDP*s could be fitted with a single curve.

species. Data in Fig. 1 *B* were generated using *PDP II*, whereas those in Fig. 1 *C* were obtained from *PDP III*. The two restitution portraits are qualitatively similar, and three different aspects of cardiac dynamics are distinguished in both at each BCL: 1), APD accommodation, which is measured during step I of PDP (*black dots*) and represents the slow change in APD after a step change in BCL. All these responses lie along the BCL line described by the equation APD + DI = BCL (*solid black line*), and whose slope is equal to −1. 2), Dynamic RC, representing steady-state responses (*blue*), which are measured during step II of PDP for a wide range of BCLs. At each BCL, the mean values of the APD and DI during step II were calculated and considered as steady-state responses at a given BCL. Steady-state responses at different BCLs form the dynamic RC. 3), Local S1-S2 RCs at each BCL, representing responses after perturbations (*purple*). These responses are measured during steps II, III, and V of PDP.

For comparison, conventional S1-S2 RCs recorded for different values of S1 (S1 = 900 ms and 500 ms) are shown in Fig. 1 *C*.

The influence of pacing history on steady-state responses

We investigated the influence of pacing history on steady-state response for isolated rabbit myocytes by applying two different modification of *PDP*: *PDP I*, where steady state was not attended at each value of BCL, and *PDP II*, where steady state was achieved at each BCL. Fig. 2 *A* presents the mean dynamic RCs for these two cases. The mean dynamic RC for guinea pig isolated cardiac myocytes obtained using *PDP III* is also plotted for comparison. It is clear from Fig. 2 *A* that APDs measured using *PDP II* are smaller than when measured using *PDP I*, showing the importance of APD accommodation. Specifically, a change in pacing history may result in up to 50% change in APD, depending on BCL. Note that 150 stimuli applied during PDP I were insufficient to reach steady state in the case of isolated rabbit myocytes.

Time constant of APD accommodation

The APD accommodation, the slow change in APD after step changes in BCLs, was observed in both isolated rabbit and guinea pig cardiac ventricular myocytes. To find the time constant, τ, of APD accommodation, data for the lower BCL were fitted with an exponential function of the form $APD = a + b \times \mathrm{Exp}[-t/\tau]$, where t is the time elapsed since the step change in BCL. Fig. 2 *B* shows τ as a function of BCL for both rabbit and guinea pig myocytes. Clearly, τ is a linear function of BCL for both species but is much smaller for guinea pig than for rabbit myocytes at all BCLs ($p < 0.05$). These results demonstrate that the steady state is achieved

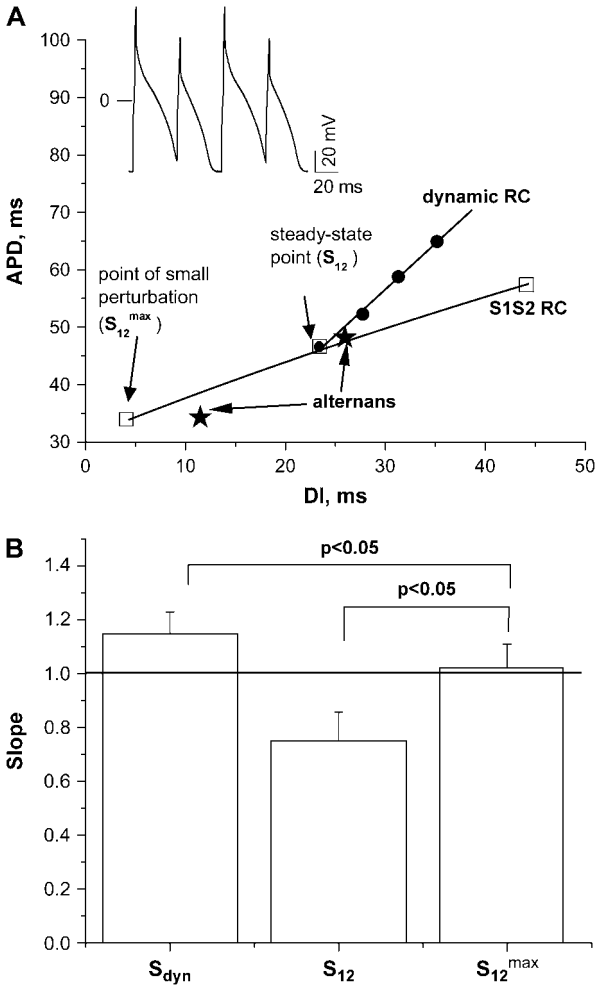

FIGURE 4 (*A*) Segment of the restitution portrait showing transition between 1:1 responses and alternans: dynamic RC (*solid circles*), local *S1-S2* RC for the shortest BCL (*open squares*), stable alternans (*stars*). (*Inset*) Traces of APs for the stable alternans. (*B*) Values of different slopes measured at the onset of alternans: S_{dyn} and S_{12} were measured at the steady-state point, and S_{12}^{max} was measured at the point of small perturbation (*A*).

faster, and thus the influence of pacing history on the dynamics is smaller for guinea pig than for rabbit myocytes.

Slopes of different RCs in the restitution portrait

Two different RCs are present in a given restitution portrait at each value of BCL: the dynamic RC and the local *S1-S2* RCs. The following procedure and assumptions enabled the measurements of the slopes of these RCs at each BCL:

Slopes of the dynamic RC (S_{dyn}): The mean values of the 10 responses measured during step II of the PDP at each BCL were determined as steady-state points that form the dynamic RC (*blue curve* in Fig. 1, *B* and *C*). We fitted the dynamic RC with an appropriate (exponential or polynomial) function and calculated the slopes analytically at steady-state points at each BCL.

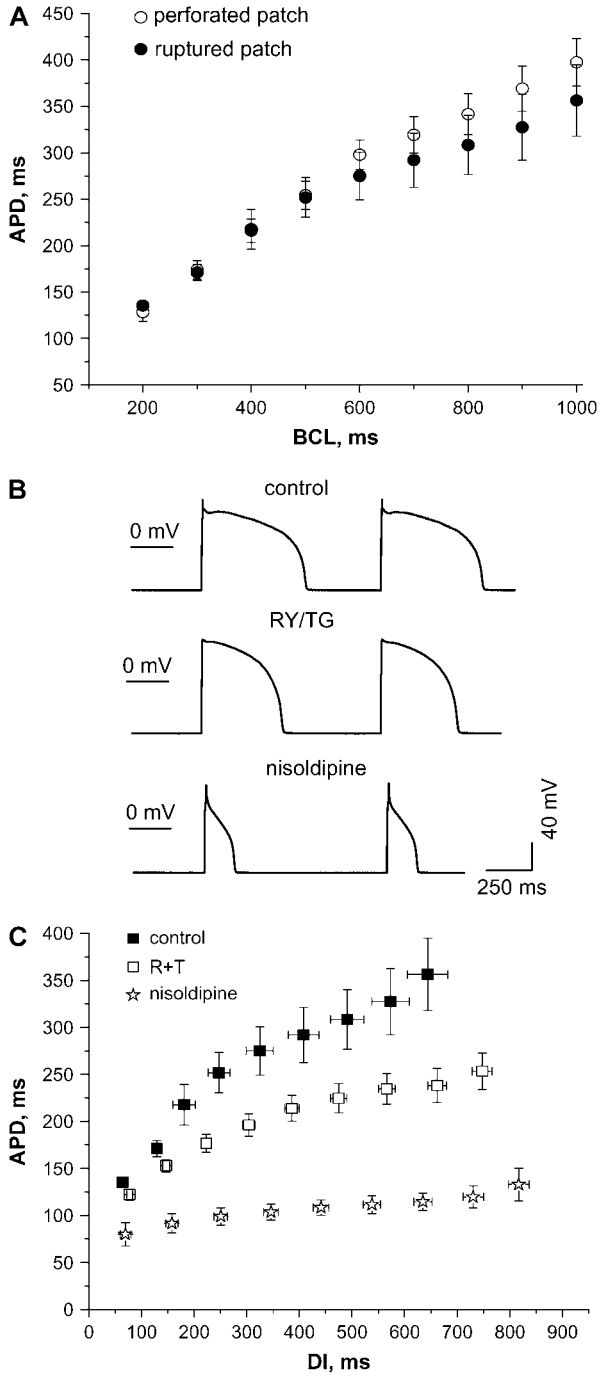

FIGURE 5 (*A*) Dynamic RCs for rabbit myocytes obtained using perforated (*open circles*) and ruptured (*solid circles*) patch techniques. Examples of AP profiles (*B*) (BCL = 1000 ms) and dynamic RCs (*C*) for rabbit myocytes obtained using perforated patch technique under control (*solid squares*), RY/TG (*open squares*), and nisoldipine (*open stars*) conditions.

Slopes of local S1-S2 RCs (S_{12}): We fitted the steady-state points and responses from steps III and V of the PDP with an appropriate function (linear or polynomial) and calculated slopes of local *S1-S2* RCs at steady-state points at each BCL.

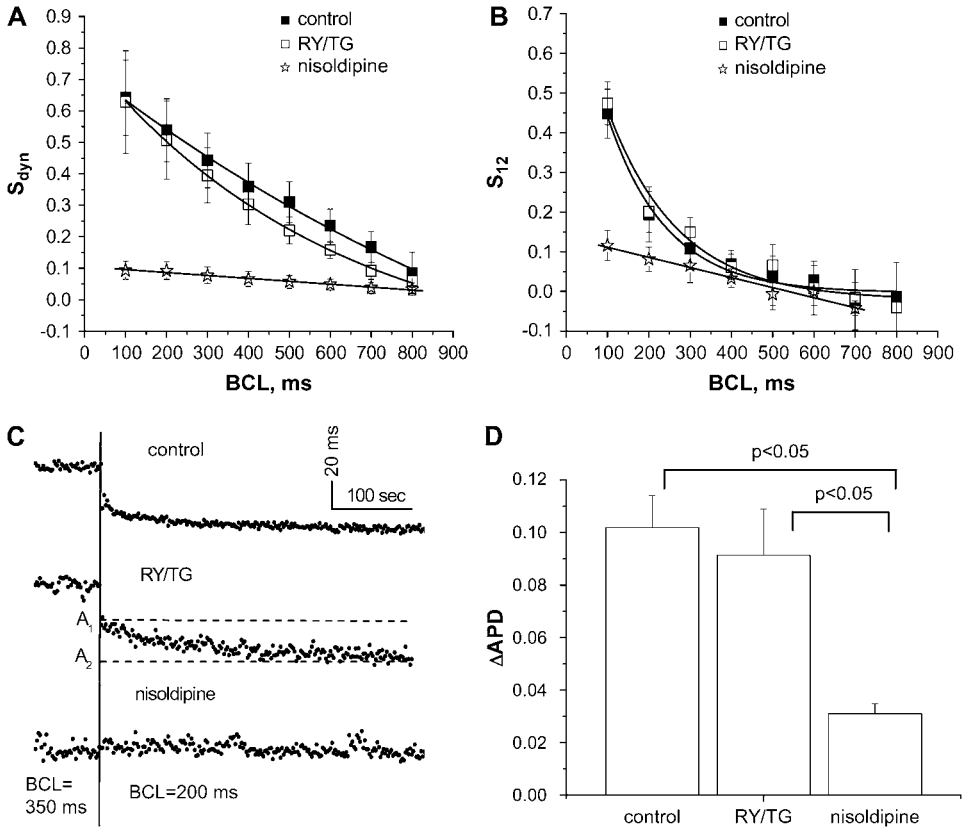

FIGURE 6 (*A*) Slopes S_{dyn}, (*B*) slopes S_{12}, and (*D*) APD measured from the restitution portraits of the rabbit myocytes (obtained using perforated patch technique) under control (*solid squares*), nisoldipine (*open stars*), and RY/TG (*open squares*) conditions. (*C*) Time course of APD accommodation under these conditions.

Slopes S_{dyn} and S_{12}: influence of pacing history

In Fig. 3 *A*, we present S_{dyn} (*solid symbols*) and S_{12} (*open symbols*) measured from the restitution portrait of the isolated rabbit ventricular myocyte as functions of BCL. We used two modifications of PDP, *PDP I* (*squares*) and *PDP II* (*circles*) (see Methods), to investigate the influence of pacing history on the slopes. For both modifications, the slopes S_{dyn} are linear functions, and S_{12} are exponential functions of BCL. Hence pacing history dramatically affects both slopes: S_{dyn} and S_{12} are smaller for *PDP II*, where steady state is achieved at each BCL. Fig. 3 *B* presents the influence of pacing history on the relationship between S_{12} and S_{dyn} (same data as in Fig. 3 *A*). There was no significant difference between data obtained using *PDP I* (*solid circles*) and *PDP II* (*open circles*). Therefore all data were fitted by a single exponential function ($S_{12} = -0.13 + 0.06\exp[S_{dyn}/0.31]$), which shows that, unlike the individual values of S_{12} and S_{dyn} (Fig. 3 *A*), the relationship between these slopes (Fig. 3 *B*) does not depend on pacing history. In Fig. 3 *C*, we show slopes S_{dyn} (*solid circles*) and S_{12} (*open circles*) measured in the restitution portrait of a guinea pig myocyte at different values of BCL. Both slopes are exponential functions of BCL. In Fig. 3 *D*, the relation between S_{12} and S_{dyn} (same data as in Fig. 3 *C*) is fitted with an exponential function ($S_{12} = -0.04 + 0.03\exp[S_{dyn}/0.275]$). Our results demonstrate quantitative but not qualitative differences in the relationships between S_{12} and S_{dyn} for both species (Fig. 3, *B* and *D*). Thus, overall, the dynamic behavior of the different slopes in the restitution portrait is clearly species independent.

Prediction of alternans

An important aim of our study was to investigate the ability of the slopes of different RCs measured in the restitution portrait to predict the onset of alternans. We observed two types of steady-state responses during step II of the PDP: stable 1:1 responses and alternans. During stable 1:1 responses, there was a single steady-state value of APD whereas during alternans APD alternated between two different values. It is generally believed that an RC slope equal to one predicts the transition between these two states (6,7). To achieve the onset of alternans very accurately, we designed a specific pacing protocol (*PDP IV*) to allow the measurement of slopes of different RCs at the onset of alternans. From a total $n = 30$ myocytes from five guinea pigs, we obtained $n = 6$ cases of stable alternans (lasting at least 60 s).

In Fig. 4 *A* the transition between 1:1 responses (*solid circles*) and alternans (*stars*) is demonstrated for the isolated guinea pig myocytes. The inset shows representative traces of APDs for stable alternans, and the local S1-S2 RC (*open squares*) is presented for the shortest BCL during 1:1

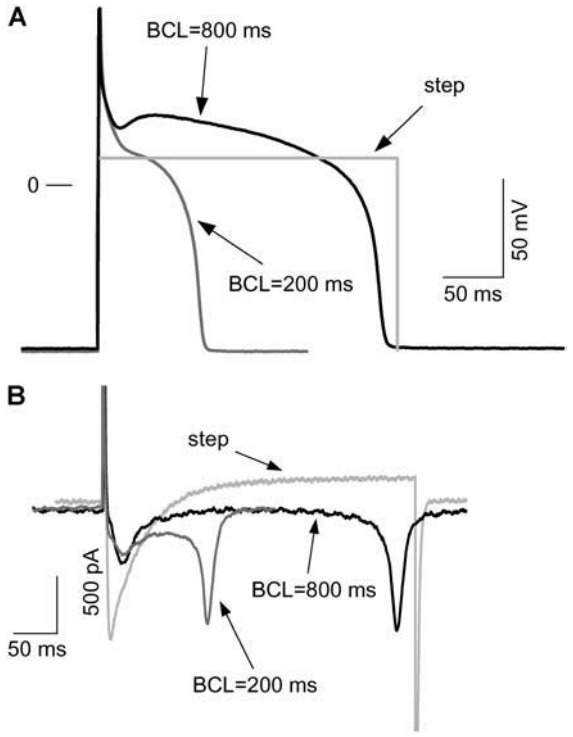

FIGURE 7 (*A*) Representative AP profiles for BCL = 800 and 200 ms, and step pulse that were used to measure peak I_{Ca}. (*B*) Peak I_{Ca} measurements under these conditions.

responses. We used two points from Fig. 4 *A* to calculate the slopes of different RCs at the onset of alternans: 1), steady-state point (where the dynamic RC intersects with S1-S2 RC); and 2), point of small perturbation for S1-S2 RC, which is also the first point after step change in BCL. We calculated slopes S_{dyn} and S_{12} at steady-state points for the shortest BCL, as described above. In addition, we measured the maximal slope of local *S1-S2* RC, S_{12}^{max}, for the shortest value of BCL at the point of small perturbation. Note that S_{12} is different from S_{12}^{max} because local *S1-S2* RCs for small BCLs are usually curved rather than linear. Fig. 4 *B* presents average values for all three slopes measured at the onset of stable alternans in guinea pig myocytes. The horizontal line at slope = 1 shows the standard restitution condition for alternans (6,7). It is clear that S_{12}^{max} predicts the onset of alternans unlike the other two slopes. Our statistical analysis shows that there are significant differences between S_{12}^{max}, S_{dyn}, and S_{12} ($p < 0.05$). Overall, our results indicate that slope S_{12}^{max} does predict the onset of alternans.

Part 2: ionic mechanism: the role of calcium current

The effect of calcium current on the restitution portrait

It is well known that the L-type calcium current ($I_{Ca\text{-}L}$) is an important determinant of the plateau phase of the AP and that it contributes to rate-dependent changes of APs in ventricular myocytes from human (27) and other species. Also, it has been suggested that intracellular Ca^{2+} cycling may contribute to differences between dynamic and *S1-S2* RCs (28) in rabbit ventricular myocytes.

To investigate the role of $I_{Ca\text{-}L}$ and intracellular Ca^{2+} cycling on different aspects of cardiac dynamics in the restitution portrait, we used the following procedures (27,28). First, to investigate the particular role of $I_{Ca\text{-}L}$ on the restitution portrait, we blocked this current using nisoldipine (1 μmol/L). Second, to test the effects of intracellular Ca^{2+} cycling on different aspects of cardiac dynamics, cells were incubated (10 min) in Tyrode's solution containing thapsigargin (TG) (200 nmol/L) and ryanodine (RY) (10 μmol/L) (RY/TG conditions) (28), during repetitive pacing at 1 Hz. The restitution portraits were recorded using *PDP I* for normal (5 rabbits, 10 cells), RY/TG (5 rabbits, 8 cells), and nisoldipine (5 rabbits, 8 cells) conditions. For our study, we used perforated patch technique instead of ruptured patch to produce minimal perturbations to the intracellular compartment. Fig. 5 *A* illustrates that the different types of techniques do not affect the dynamic RCs. Typical traces of AP (BCL = 1000 ms) and dynamic RCs recorded using perforated patch technique under control, RY/TG, and nisoldipine conditions are shown in Fig. 5, *B* and *C*. Note that blockage of intracellular Ca^{2+} cycling reduces APDs at all values of BCLs ($p < 0.05$), and this effect is more pronounced if $I_{Ca\text{-}L}$ is abolished.

Slopes of different RCs (S_{dyn} and S_{12}) and τ were measured at different values of BCL as was described above. Fig. 6 depicts the slopes S_{dyn} (*panel A*) and S_{12} (*panel B*) under control (*solid squares*), nisoldipine (*open stars*), and RY/TG (*open squares*) conditions. Note that S_{dyn} changed significantly ($p < 0.05$) from the control case for all values of BCL under nisoldipine condition. At the same time, S_{12} changed significantly ($p < 0.05$) from the control case only at small values of BCLs. Note also in Fig. 6, *A* and *B*, that RY/TG superfusion had no significant effect on either slope S_{dyn} (*panel A*) or S_{12} (*panel B*) at any BCL. These results demonstrate the importance of $I_{Ca\text{-}L}$, but not intracellular Ca^{2+} cycling, on the frequency-dependent behavior of periodically paced cardiac myocytes.

Typical time courses of APD accommodation after abrupt changes of BCL from 350 ms to 200 ms under control, RY/TG, and nisoldipine conditions are shown in Fig. 6 *C*. In Fig. 6 *C*, APD accommodation under control and RY/TG conditions and the absence of APD accommodation during superfusion of nisoldipine are similar for all values of BCL. Note that APD accommodation effect could be described as an exponential function of time under control and RY/TG cases. On the contrary, after blocking $I_{Ca\text{-}L}$ the APD upon changing the BCL is no longer an exponential function of time. Thus, to determine the influence of the calcium current on APD accommodation, we introduced a new parameter, ΔAPD, instead of the time constant τ. We define $\Delta APD = 1 - A_2/A_1$, where A_1, A_2 are the mean values of the first and

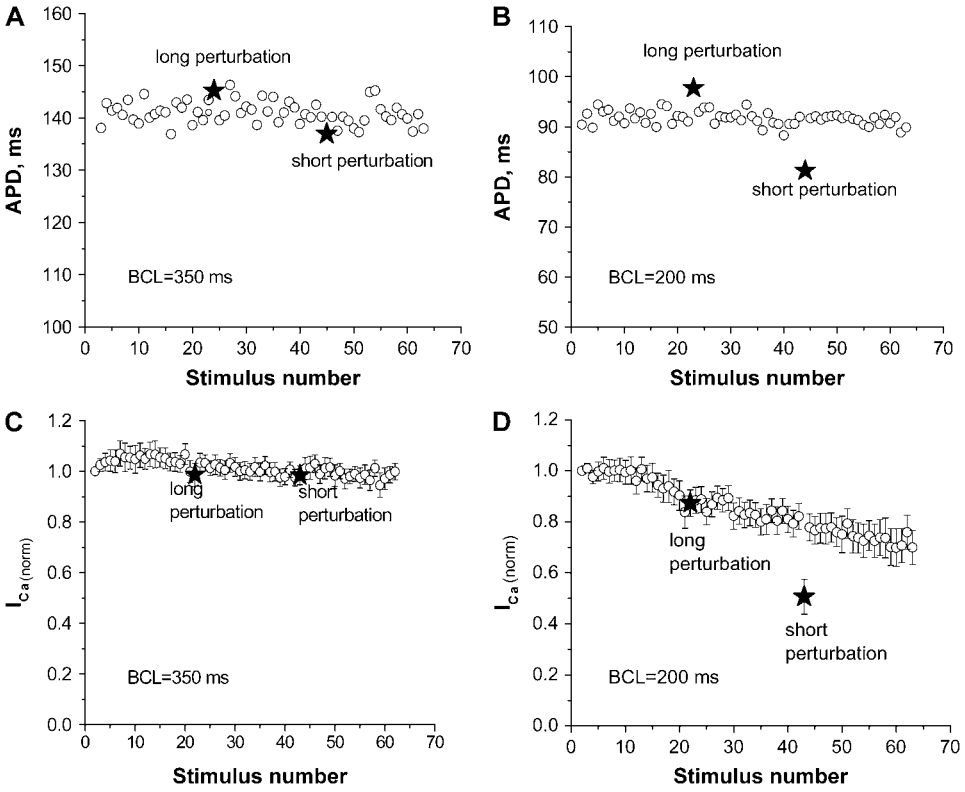

FIGURE 8 AP clamp peak I_{Ca} measurements. APDs from the restitution portrait recorded for BCL = 350 ms (*A*) and 200 ms (*B*) using steps II–VI of *PDP II*. (*C*) Normalized peak I_{Ca} at BCL = 350 ms. (*D*) Normalized peak I_{Ca} at BCL = 200 ms.

last 10 APDs at any given value of BCL. Fig. 6 *D* shows the mean values of ΔAPD calculated under control, nisoldipine, and RY/TG conditions at BCL = 200 ms. These results indicate that in the absence of $I_{Ca\text{-}L}$ the APD accommodation effect disappears ($p < 0.05$). In contrast, the role of intracellular calcium cycling appears insignificant.

Measurements of peak calcium current, I_{Ca}

We measured peak I_{Ca} under voltage-clamp conditions using both APs profiles and step pulses recorded at different values of BCLs (see Methods). Representative traces of single step pulse and AP profiles recorded for BCL = 800 and 200 ms are presented in Fig. 7 *A*. The traces of I_{Ca} under these conditions are shown in Fig. 7 *B*. Peak I_{Ca} was measured as the difference between holding current and peak inward current.

The role of peak I_{Ca} in the restitution portrait: response to perturbations

An important aspect of cardiac dynamics revealed by the restitution portrait is the difference between the dynamic and the *S1-S2* RCs at each value of BCL due to short-term memory effects (see Fig. 1). Using the restitution portrait enables the determination of the role of I_{Ca} in this aspect through the analysis of I_{Ca} changes during steady-state stimulation (dynamic RC) and after the long and short perturbations in BCL (local *S1-S2* RCs).

Since our initial results indicated that $I_{Ca\text{-}L}$ played a major role in determining the slopes S_{dyn} and S_{12}, we decided to examine the role of the peak I_{Ca} in detail. We combined the use of the restitution portrait and AP clamp techniques to measure peak I_{Ca} during steady-state stimulation (dynamic RC) as well as after long and short perturbations in BCL (local *S1-S2* RCs). We measured the peak I_{Ca} under AP-clamp conditions using segments of restitution portraits for different values of BCL (see Methods). As an example, in Fig. 8, *A* and *B*, we have plotted 63 consecutive APDs from the restitution portrait recorded for BCL = 350 and 200 ms, respectively, using steps II–VI of *PDP II*. Note that for large values of BCL (≥350 ms), APDs for the long and short perturbations are not significantly different from the steady-state values. Thus, both perturbations lead to change in DIs. In contrast, for BCL = 200 ms, long and short perturbations lead to differences in both APD and DI. The peak I_{Ca} was measured in each trial for different BCLs (800, 650, 500, 350, and 200 ms). In Fig. 8, *C* and *D*, we present the mean peak I_{Ca} normalized to the first value for BCLs 350 and 200 ms, respectively. The stars depict the normalized peak I_{Ca} during long and short perturbations in BCL. Data for BCLs 500, 650, and 800 ms are qualitatively similar to those for 350 ms (not shown). The data demonstrate that peak I_{Ca} does not change in response to the perturbations for large values of BCL (≥350 ms). However, peak I_{Ca} is significantly smaller in response to short perturbation for BCL = 200 ms.

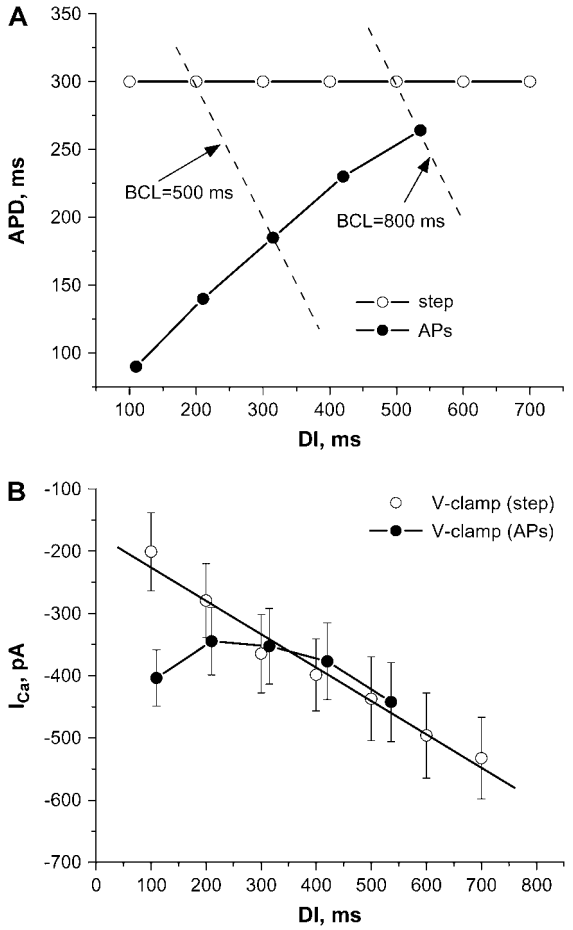

FIGURE 9 (*A*) Durations of APs and step pulse as functions of DIs for conventional voltage-clamp step protocol (*open circles*) and for APs voltage-clamp protocols (*solid circles*). Broken lines represent equal BCLs for 800 and 500 ms. (*B*) Peak I_{Ca} recorded during step (*open circles*) and APs (*solid circles*) voltage-clamp protocols.

These results indicate that the peak I_{Ca} is responsible for the difference between the dynamic and the *S1-S2* RCs only at small values of BCL.

The role of peak I_{Ca} in the restitution portraits: frequency dependence

Data from the previous section demonstrated that peak I_{Ca} plays a significant role in the restitution portrait only at small values of BCL. To investigate whether this is due to changes in AP profile at different BCLs, we measured peak I_{Ca} using conventional voltage-clamp step protocol with different time intervals (corresponding to DI) between steps.

Fig. 9 *A* illustrates the difference between conventional voltage-clamp step protocol (*open circles*) and AP clamp protocol (*solid circles*) as BCL decreases. Fig. 9 *B* shows peak I_{Ca} recorded using both these techniques. In the step protocol, as BCL decreases the step duration remains the same, and only time intervals between steps decreases, allowing the measurement of frequency-dependent reactivation kinetics of peak I_{Ca}. The peak I_{Ca} (Fig. 9 *B*) decreases (in absolute value) as DI decreases, indicating a lack of full reactivation of I_{Ca} at higher frequencies. In the AP clamp, as BCL decreases, both APDs and DIs changed with frequency allowing the measurement of both frequency-dependent reactivation and inactivation kinetics of I_{Ca} in the restitution portrait. Peak I_{Ca} measured using AP clamp decreases as DI decreases up to 300 ms and then increases again, suggesting interplay between reactivation and inactivation kinetics of I_{Ca} at high frequencies. An interplay between reactivation and inactivation kinetics at higher frequencies might explain results from the previous section indicating that peak I_{Ca} plays a significant role in the restitution portrait at small values of BCL (Fig. 8 *C*).

DISCUSSION

We have utilized the single cell restitution portrait model to begin the characterization of ionic mechanisms underlying the complex phenomena that control heart rate dependence of the APD. Our results show that restitution portraits of isolated guinea pig and rabbit myocytes are qualitatively similar to those seen previously in numerical experiments and in small pieces of bullfrog ventricular muscle (17). In all cases, three different aspects of cardiac dynamics are present at each value of BCL: 1), APD accommodation (i.e., the time necessary for APD to reach a steady state); 2), steady-state responses that form the dynamic RC; and 3), the responses to perturbations that form the local *S1-S2* RCs at each BCL. Overall the data suggest that the restitution portrait is a fundamental characteristic of excitation of the myocardial cell, rather than the result of structural complexities of the multi-cellular cardiac tissue. Determining how such complexities affect the restitution portrait will require comparing the single cell data with similar data derived from experiments in the intact mammalian heart.

Another major objective of our study was to determine the time constant, τ, of APD accommodation as one of the important parameters controlling the dynamics of the periodically paced cardiac myocyte. To our knowledge, this is the first set of measurements of τ at a wide range of BCLs. All previous measurements (10,17,29) of τ were made only for one or several values of BCL. Our data demonstrate that τ is a linear function of BCL for both rabbit and guinea pig cardiac ventricular myocytes. The results show also that τ is much smaller for the guinea pig than for the rabbit for all BCLs, which indicates the ability of the guinea pig myocyte to reach steady state in a shorter period of time. The different values of τ for guinea pig and rabbit cardiac myocytes might be due to different ionic currents in these species or different kinetics of the same currents. However, this issue is beyond the scope of our study and will require further investigation.

We investigated the influence of pacing history on the slopes of different types of RC, S_{dyn}, and S_{12} in the restitution portraits. In particular, we applied two modifications of the PDP to the isolated rabbit myocyte: one that did and another that did not allow reaching a steady state at each BCL. In both species S_{dyn} and S_{12} strongly depend on pacing history; they both increase with decreasing BCL. However, the relationship between these slopes is a generic feature of the species and is independent of pacing history.

We also examined the ability of the slopes of different RCs measured in the restitution portrait to predict the onset of alternans. According to the restitution condition (6,7) the slope of the RC must be equal to 1 at the onset of alternans. Previously it was demonstrated that this condition is not achieved in many situations, in particular, stable 1:1 behavior was observed when the slope of RC was >1 (9,12,13) or the transition to alternans occurred in the presence of a shallow RC (14,15). In our experiments, the onset of stable alternans was determined very accurately through a unique pacing protocol, which also allowed measurements of the slopes of different RCs at the shortest possible BCL yielding a 1:1 response. Specifically, we measured S_{dyn} and S_{12} at steady-state points and the maximal slope S_{12}^{max} at the point of small perturbation. Previous results (17) demonstrated that S_{12}^{max} predicts the onset of alternans in bullfrog myocardium. However these results needed confirmation in mammalian myocytes. Our results indicate that S_{12}^{max} does predict the onset of alternans in isolated guinea pig myocytes more accurately than can other slopes ($r < 0.05$). Note that slope S_{12}^{max} measured in our experiments is different from the commonly measured S_{12} slope (11,15,28).

Using nisoldipine in some experiments and ryanodine and thapsigargin in others, we investigated the separate roles of L-type calcium current and intracellular Ca^{2+} cycling in the restitution portrait. Our results indicate that $I_{Ca\text{-}L}$ is important in the mechanisms of different aspects of cardiac dynamics in the restitution portrait. More specifically, $I_{Ca\text{-}L}$ dramatically affects the slopes S_{dyn} and S_{12} and also APD accommodation. Note that the $I_{Ca\text{-}L}$ significantly affects S_{dyn} at different values of BCL, but it affects S_{12} only at small values of BCL. In contrast, our results indicate that intracellular Ca^{2+} cycling did not affect in any significant way either the slopes S_{dyn} and S_{12} or APD accommodation. The latter result seems to be at odds with results from the literature (28) showing a major influence of intracellular Ca^{2+} cycling on the maximal slopes of S_{dyn} and S_{12}. There are several possible explanations for such a discrepancy. One possibility is that, unlike the investigation by Goldhaber et al. (28) who applied only 10 beats at each BCL, we measured S_{dyn} while ensuring that steady sate was achieved at each BCL. This process might indeed take several minutes. Moreover, the maximal slope of S_{dyn} measured by Goldhaber et al. included not only APDs recorded during 1:1 responses (what usually is used to construct the dynamic RC) but also the APDs during alternans (which we did not include in our measurements). Recall that our results indicate that pacing history affects dramatically the slopes of different RCs. This also could be the reason intracellular Ca^{2+} cycling affected S_{dyn} in Goldhaber et al. but not in our experiments. In addition, the measurement of S_{12} is also very different in our experiments: we measured local S_{12} over many values of BCL (S1), whereas S1 = 400 ms in Goldhaber et al.

Although $I_{Ca\text{-}L}$ affects significantly slopes S_{dyn} and S_{12} at different values of BCLs, the results of the AP clamp experiments demonstrate that the peak I_{Ca} does not change in response to the perturbations for the large values of BCL ($\geq$350 ms). However, the peak I_{Ca} is significantly smaller when considering the small perturbation for BCL = 200 ms. These results indicate that the peak I_{Ca} plays a significant role in frequency dependence of the slopes S_{dyn} and S_{12} only at small values of BCL. Our further investigations indicate that this effect is most probably caused by the size and/or shape of the applied AP profile at high frequencies, when there is an interplay between reactivation and inactivation kinetics.

Thus, the L-type calcium current plays a crucial role in multiple aspects of cardiac dynamics in the restitution portrait. Specifically, in the absence of $I_{Ca\text{-}L}$ there is no APD accommodation or frequency dependence of the slopes. However, our data clearly show that neither intracellular Ca^{2+} cycling nor peak I_{Ca} is responsible for these phenomena. The exact mechanism of it is still unclear and several possibilities need to be considered. For example, accumulation of calcium ions with time might affect the inactivation of calcium channels, which will lead to APD accommodation and frequency dependence of slopes. In addition, $I_{Ca\text{-}L}$ might affect other currents (through potassium channels, sodium-calcium exchanger, etc.) and cause these effects.

In summary, we systematically analyzed restitution portraits of isolated cardiac myocytes obtained from two different mammalian species—the rabbit and the guinea pig. We characterized various aspects of the cardiac dynamics and the role of calcium current and intracellular calcium cycling in the restitution portrait. We demonstrated that $I_{Ca\text{-}L}$ dramatically affected APD accommodation and the individual slopes of dynamic and *S1-S2* RCs measured in the restitution portrait. Furthermore, peak I_{Ca} plays a role only at small values of BCL, whereas intracellular Ca^{2+} cycling does not play any significant role in the restitution portrait. In conclusion, we have shown that the restitution portrait is a powerful technique to investigate the restitution properties of periodically paced cardiac myocytes, and the onset of alternans, in particular. We also demonstrated that the calcium current plays a crucial role in the restitution portrait.

We acknowledge the technical help of Arkadzi Talkachou.

This work was supported by Heart Rhythm Society postdoctoral Fellowships 2004 and 2005 (E.G.T.) and by grants from National Heart, Lung, and Blood Institute (P01-HL39707; R01-HL70074; R01-HL60843 to J.J.).

REFERENCES

1. Karma, A. 1994. Electrical alternans and spiral wave breakup in cardiac tissue. *Chaos*. 4:461–472.
2. Watanabe, M. A., N. F. Otani, and R. F. Gilmour Jr. 1995. Biphasic restitution of action potential duration and complex dynamics in ventricular myocardium. *Circ. Res.* 76:915–921.
3. Gilmour, R. F. Jr., and D. R. Chialvo. 1999. Editorial: Electrical restitution, critical mass and the riddle of fibrillation. *J. Cardiovasc. Electrophysiol.* 10:1087–1089.
4. Fox, J. J., R. F. Gilmour Jr., and E. Bodenschatz. 2002. Conduction block in one-dimensional heart fibers. *Phys. Rev. Lett.* 89:198101.
5. Fenton, F. H., E. M. Cherry, H. M. Hastings, and S. J. Evans. 2002. Multiple mechanisms of spiral wave breakup in a model of cardiac electrical activity. *Chaos*. 12:852–892.
6. Nolasco, J. B., and R. W. Dahlen. 1968. A graphic method for the study of alternation in cardiac action potentials. *J. Appl. Physiol.* 25: 191–196.
7. Guevara, M., G. Ward, and L. Glass. 1984. Electrical alternans and period-doubling bifurcations. *In Proc Comput. Cardiol.* K. Ripley, editor. IEEE Computer Society Press, Washington, DC. 167–170.
8. Shivkumar, K., and J. N. Weiss. 2004. The slippery slope of human ventricular arrhythmias. *J. Cardiovasc. Electropyhsiol.* 15:1364–1365.
9. Hall, G. M., S. Bahar, and D. J. Gauthier. 1999. Prevalence of rate-dependent behaviors in cardiac muscle. *Phys. Rev. Lett.* 82:2995–2998.
10. Elharrar, V., and B. Surawicz. 1983. Cycle length effect on restitution of action potential duration in dog cardiac fibers. *Am. J. Physiol.* 244: H782–H792.
11. Cherry, E. M., and F. H. Fenton. 2004. Suppression of alternans and conduction blocks despite APD restitution: electrotonic, memory and conduction velocity effects. *Am. J. Physiol.* 286:H2332–H2341.
12. Gilmour, R. F. Jr. 2002. Electrical restitution and ventricular fibrillation: negotiating a slippery slope. *J. Cardiovasc. Electropyhsiol.* 13: 1150–1151.
13. Banville, I., and R. A. Gray. 2002. Effect of action potential duration and conduction velocity restitution and their spatial dispersion on alternans and the stability of arrhythmias. *J. Cardiovasc. Electrophysiol.* 13:1141–1149.
14. Koller, M. L., M. L. Riccio, and R. F. Gilmour Jr. 1998. Dynamic restitution of action potential duration during electrical alternans and ventricular fibrillation. *Am. J. Physiol.* 275:H1635–H1642.
15. Riccio, M. L., M. L. Koller, and R. F. Gilmour Jr. 1999. Electrical restitution and spatiotemporal organization during ventricular fibrillation. *Circ. Res.* 84:955–963.
16. Tolkacheva, E. G., D. G. Schaeffer, D. J. Gauthier, and W. Krassowska. 2003. Condition for alternans and stability of the 1:1 response pattern in a ''memory'' model of paced cardiac dynamics. *Phys. Rev. E.* 67:031904.
17. Kalb, S. S., H. Dobrovolny, E. G. Tolkacheva, S. F. Idriss, W. Krassowska, and D. J. Gauthier. 2004. The restitution portrait: a new method for investigating rate-dependent restitution. *J. Cardiovasc. Electrophys.* 15:698–709.
18. Choi, B.-R., T. Liu, and G. Salama. 2004. Adaptation of cardiac action potential duration to stimulation history with random diastolic interval. *J. Cardiovasc. Electrophys.* 15:1188–1197.
19. Li, M., and N. F. Otani. 2003. Ion channel basis for alternans and memory in cardiac myocytes. *Ann. Biomed. Eng.* 31:1213–1230.
20. Fox, J. J., J. L. McHarg, and R. F. Gilmour Jr. 2002. Ionic mechanism of electrical alternans. *Am. J. Physiol. Heart. Circ. Physiol.* 282: H516–H530.
21. Simurda, J., M. Simurdova, M. Pasek, and P. Braveny. 2001. Quantitative analysis of cardiac electrical restitution. *Eur. Biophys. J.* 32: 500–514.
22. Yehia, A. R., D. Jeandupeux, F. Alonso, and M. R. Guevara. 1999. Hysteresis and bistability in the direct transition from 1:1 to 2:1 rhythm in periodically driven single ventricular cells. *Chaos*. 9:916–931.
23. Kalb, S. S., E. G. Tolkacheva, D. G. Schaeffer, D. J. Gauthier, and W. Krassowska. 2005. Restitution in mapping models with an arbitrary amount of memory. *Chaos*. 15:023701–11.
24. Feng, J., L. Yue, Zh. Wang, and S. Nattel. 1998. Ionic mechanisms of regional action potential heterogeneity in the canine right atrium. *Circ. Res.*, 83:541–551.
25. Anumonwo, J. M. B., M. Delmar, A. Vinet, D. C. Michaels, and J. Jalife. 1991. Phase resetting and entrainment of pacemaker activity in single sinus nodal cells. *Circ. Res.* 168:1138–1153.
26. Anumonwo, J. M. B., L. C. Freeman, W. M. Kwok, and R. S. Kass. 1992. Delayed rectification in single cells isolated from guinea pig sinoatrial node. *Am. J. Physiol.* 262:H921–H925.
27. Li, G. R., B. Yang, J. Feng, R. F. Bosch, M. Carrier, and S. Nattel. 1999. Transmembrane I_{Ca} contributes to rate-dependent changes of action potentials in human ventricular myocytes. *Am. J. Physiol.* 276: H98–H106.
28. Goldhaber, J. I., L.-H. Xie, T. Duong, Ch. Motter, K. Khuu, and J. N. Weiss. 2005. Action potential duration restitution and alternans in rabbit ventricular myocytes. The key role of intracellular calcium cycling. *Circ. Res.* 96:459–466.
29. Watanabe, M. A., and M. L. Koller. 2002. Mathematical analysis of dynamics of cardiac memory and accommodation: theory and experiment. *Am. J. Physiol.* 282:H1534–H1547.